Tectonophysics 723 (2018) 27–40

Contents lists available at ScienceDirect

Tectonophysics

journal homepage: www.elsevier.com/locate/tecto

Tectonic evolution of the NE section of the Pamir Plateau: New evidence from field observations and zircon U-Pb geochronology

Chuan-Lin Zhang[a,*], Hai-Bo Zou[b], Xian-Tao Ye[a], Xiang-Yan Chen[b]

[a] C[illegible] f O[illegible] n[illegible], H[illegible] i[illegible] n[illegible] si[illegible], N[illegible] 210093, PR C[illegible] in
[b] D[illegible] [illegible] n f G[illegible] s i[illegible] n[illegible] s, A[illegible] n[illegible] n[illegible] si[illegible], A[illegible] n, AL 36849-5305, [illegible]A

ARTICLE INFO

K[illegible] [illegible] s:
Pamir Plateau
Bulunkuole Group
Field observation
Zircon U-Pb age
Tectonic evolution

ABSTRACT

The Pamir Plateau at the western end of the India–Asia collision zone underwent long-term terrane drifting, accretion and collision between early Paleozoic and Mesozoic. However, the detailed evolution of this plateau, in particular, the timing of the Proto- and Palaeo-Tethys ocean subduction and closure, remains enigmatic. Here we report new field observations and zircon U-Pb ages and Hf isotopic compositions of the representative rocks from the so-called Precambrian basement in the northeastern Pamir, i.e., the Bulunkuole Group. The rock associations of the Bulunkuole Group indicate volcano-sedimentary sequences with arc affinities. Geochronological data demonstrate that the deposition age of the Bulunkuole Group in the NE section of the Pamir was Middle to Late Cambrian (530–508 Ma) rather than Paleoproterozoic. The deposition age became progressively younger from south to north. The amphibolite- to granulite facies metamorphism of the Bulunkuole Group took place at ca. 200–180 Ma. Unlike the scenario in the Southern Kunlun terrane (SKT) in the eastern section of the West Kunlun Orogenic Belt (WKOB), early Paleozoic metamorphism (ca. 440 Ma) was absent in this area. Two phases of magmatic intrusions, composed of granites and minor gabbros with arc geochemical signatures, emplaced at 510–480 Ma and 240–200 Ma. The amphibolite (meta mafic sheet? 519 Ma) and the meta-rhyolite (508 Ma) have zircon εHf(t) values of 1.6 to 5.9 and − 1.5 to 1.4, respectively. The 511 Ma gneissic granite sheet and the 486 Ma gabbro have zircon εHf(t) values of − 0.1 to 2.4 and 1.3 to 3.6, respectively. Zircon εHf(t) of the 245 Ma augen gneissic granite sheet varies from − 2.2 to 2.0 whereas the metamorphic zircons from the amphibolite (193 Ma) and high-pressure mafic granulite sample (187 Ma) have negative εHf(t) values of − 5.3 to − 2 and − 15 to − 12, respectively. In line with rock association and the deposition age of the Bulunkuole Group and the Saitula Group in the eastern section of WKOB, we propose that both of them were accretionary wedge between the Tarim and Tianshuihai terrane formed during the Proto-Tethys ocean south- southwestward subduction (pr-441.6(Tian-446.438so)NE6.43(formPamir6.435Tiandi41.63(and)not1.60a[illegible]ge[illegible]) sequences. The accretion between NE Pamir and the Central Pamir was completed by ca. 180 Ma as demonstrated by the metamorphic zircon U-Pb age of the high pressure mafic granulite in the NE Pamir.

1. Introduction

The Pamir Plateau (or Pamir Syntax) at the western end of the India–Asia collision zone underwent a protracted history of terrane drifting, accretion, and collision since early Paleozoic (or Sinian) until the final suturing and basin closure during the Mesozoic (e.g. Schwab et al., 2004; Xiao et al., 2002a, 2005; Zanchi and Gaetani, 2011; Robinson et al., 2012, 2015, 2016; Angiolini et al., 2013, 2015; Rutte et al., 2017). Gondwana-affinity crustal fragments (terranes) within the Pamir Plateau consist of the Central Pamir and Southern Pamir terranes which collided with the southern margin of Asia during the closure of the Paleo-Tethys Ocean (Pashkov and Budanov, 1990; Tapponnier et al., 1981; Burtman and Molnar, 1993; Yin and Harrison, 2000; Burtman, 2010). However, recent studies have identified early Paleozoic orogenic event in the eastern section of the Western Kunlun Orogenic Belt (WKOB), as demonstrated by the Cambrian Kudi-Qimanyute ophiolite between the Northern Kunlun terrane (NKT) and the Southern Kunlun terrane (SKT) (Pan and Wang, 1994; Pan, 1996; Matte et al.,

* Corresponding author.
E-[illegible] i[illegible] [illegible]ss: zhangchuanlin@hhu.edu.cn (C.-L. Zhang).

https://doi.org/10.1016/j.tecto.2017.11.036
Received 6 April 2017; Received in revised form 23 November 2017; Accepted 27 November 2017
Available online 02 December 2017
0040-1951/

1996; Mattern and Schneider, 2000; Xiao et al., 2002a; Zhang et al., 2004), the early Paleozoic metamorphism in SKT (Zhou et al., 1999, 2000; Zhang et al., 2017), and the widespread late Devonian red molasse unconformably overlying on the Pre-Devonian sequences both in SKT and NKT (Xinjiang BGMR, 1993; Mattern and Schneider, 2000). Several important questions remain unanswered regarding the tectonics of the eastern section of the Pamir Plateau including: (1) correlation and continuity of early Paleozoic suture zones and tectonic terranes along strike, especially in regard to possible equivalences in WKOB to the west; (2) precise tectonic evolution stages and geodynamic background prior to the Mesozoic collision with the Asian plate.

In recent years, local geologists accomplished 1/250,000 and some 1/5000 geological mapping of the WKOB and their works significantly improved our geological knowledge of this enigmatic tectonic unit (Han et al., 2001, 2002, 2004; Ji et al., 2004, 2011; Cui et al., 2006a, 2006b). Based on these fundamental data, we revisit the pre-Mesozoic evolution of the NE Pamir. In this contribution, we report our new field observations in NE Pamir. Systematic zircon U-Pb dating and Lu-Hf isotope analysis were also carried out for selected key rock types. Our new observations and data contribute to the current understanding of the early Paleozoic accretion process, the Cimmerian orogeny, and the tectonic evolution prior to late Mesozoic in this region, and highlight important questions regarding the pre-Mesozoic amalgamation history between the Eurasia continent and the Gondwanan fragments of the Pamir Plateau.

2. Regional geology

The Pamir salient has generally been divided into three tectonic units, i.e., the Northern Pamir, Central Pamir, and Southern Pamir (Fig. 1) (Burtman and Molnar, 1993; Schwab et al., 2004; Robinson et al., 2007, 2016; Angiolini et al., 2015). The Northern Pamir was interpreted as a composite Paleozoic arc terrane correlative to the NKT-SKT of the WKOB (Tapponnier et al., 1981; Boulin, 1988; Burtman and Molnar, 1993; Yin and Harrison, 2000) or a Triassic accretion complex (Schwab et al., 2004; Robinson et al., 2012). However, our recent studies did not favor this correlation. The NKT and SKT underwent distinct early Paleozoic metamorphism whereas no early Paleozoic metamorphism was identified in the Northern Pamir, at least in the Chinese NE Pamir (see following discussions) (Y. Zhang et al., 2016; Zhang et al., 2017). The correlation of the Central Pamir terrane to other tectonic units in eastern WKOB remains puzzling. The Central Pamir terrane was regarded as (1) a separate terrane without any direct correlative body in Tibet (e.g., Burtman and Molnar, 1993; Robinson, 2009), (2) the equivalent to the Mazar-Songpan-Ganzi terrane (Yin and Harrison, 2000; Robinson et al., 2004), or (3) the equivalent to the Qiangtang terrane (Schwab et al., 2004; Valli et al., 2008). The

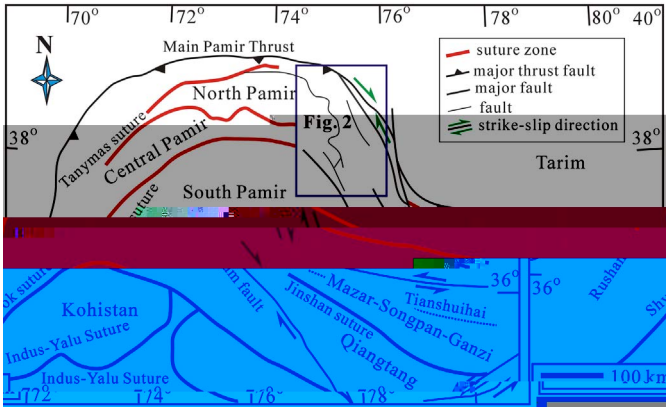

Fig. 1. (a) Simplified tectonic map of the western end of the Himalayan-Tibetan orogen showing the major tectonic terranes.
(Modified after Robinson et al., 2012).

Southern Pamir-Karakoram terrane is generally interpreted to be continuous, although they may be separated by a suture zone or a region of highly attenuated continental crust from Paleozoic rifting (Fig. 1, Zanchi et al., 2000). Thus, although the three tectonic units (Northern Pamir, Central Pamir, and Southern Pamir) are widely accepted by geologists, the boundaries between these tectonic units, at least in the NE Pamir, remain foggy. This is why the division lines between the three distinct units in the NE Pamir are not clearly shown in many previous studies (e.g., Schwab et al., 2004; Valli et al., 2008; Robinson et al., 2012).

While it has been suggested that the Central and Northern Pamir amalgamated along the Mesozoic Tanymas suture zone in Tajikistan (Angiolini et al., 2013, 2015; Robinson et al., 2012), this suture zone is not well defined in the eastern Chinese Pamir, in spite of the identification of the high-pressure mafic granulite to the north of the Tashkorgon County (Fig. 2) (Qu et al., 2007; Yang et al., 2010). In fact, this section is dominated by the Muztaghata gneiss dome and Kongur Shan gneiss dome, locally termed as the Bulunkuole Group. This group was believed to be a Precambrian basement and equivalent to the Saitula Group, as the Precambrian basement of the SKT in the eastern section of WKOB (Fig. 1) (Qu et al., 2007; Ji et al., 2004). Geological mapping shows that the rock associations and metamorphic features on the north and south sides of the high-pressure mafic granulite resemble each other (Zhang et al., 2003, Yang et al., 2011; Ji et al., 2011). In combination with the absence of ophiolites, this high-pressure mafic granulite might not represent the eastern continuous extension of the Tanymas suture zone.

3. Field observations and sample descriptions

The Bulunkuole Group is distributed along the Kongur –Muztaghata domain with an area 200 km long and 5–50 km wide in N-S direction, according to the 1/250,000 geologic map (Fig. 2). This group was intruded by the Triassic Kongur granodiorite-granite pluton (ca. 1200 km^2) in the west and by the early Paleozoic Datong granite pluton (ca. 800 km^2) in the east (Jiang et al., 1999, 2002). Based on 1/50,000 mappings and our own field observations, we describe the rock associations, stratigraphic and metamorphic features in the following three key areas: the Zankan-Laobing iron deposit area (south, Fig. 3), the Wazelapu area (to south of the high-pressure mafic granulite location, central, Fig. 4) and the Ziluoyi iron deposit area (north) (Fig. 5).

The Zankan-Laobing area has been studied extensively in recent years due to the presence of large BIF-type iron deposits (Chen et al., 2013 and references therein). To southwest the Bulunkuole Group is in contact with a newly identified Archean- Mesoproterozoic Mazaer Complex by a NW-strike fault (Fig. 3, Ji et al., 2011 and our unpublished data, as the Precambrian basement of the Southern Pamir). In this section, the Bulunkuole Group was intruded by Mesozoic and Cenozoic granites and un-conformably covered by the Cretaceous red molasse (Fig. 3). The strata strike to NW300°–330° and dip NE at an angle of 30° to 50°. In most outcrops, the original sedimentary bedding was well preserved, in spite of amphibolite-facies metamorphism. The main rocks in this area comprise garnet-bearing schist (gneiss), biotite schist, quartzite, biotite plagioclase-quartz leptynite (meta-rhyolite), amphibolite (meta-basalts) (Fig. 6a, b), magnetite layers (Fig. 6a) and minor marble. Geological section survey revealed that the volcanic rocks (meta-rhyolites and meta-basalts) account for ca. 30% while the sedimentary rocks account for ca. 70% in thickness. The magnetite layers (or lens) mostly occur between amphibolite (meta-basalt) or bimodal volcanic sequence (composed of amphibolite and feldspar-quartz leptynite) and biotite schist or quartzite. These magnetite layers include hornblende-bearing magnetite, quartz magnetite, biotite magnetite and barite-oulopholite magnetite (Fig. 6a, Chen et al., 2013), showing typical BIF-type iron deposit signatures (Hu et al., 2016).

The central section of the Bulunkuole Group is intruded by early Paleozoic and Mesozoic granites (Fig. 4). The strata strike to

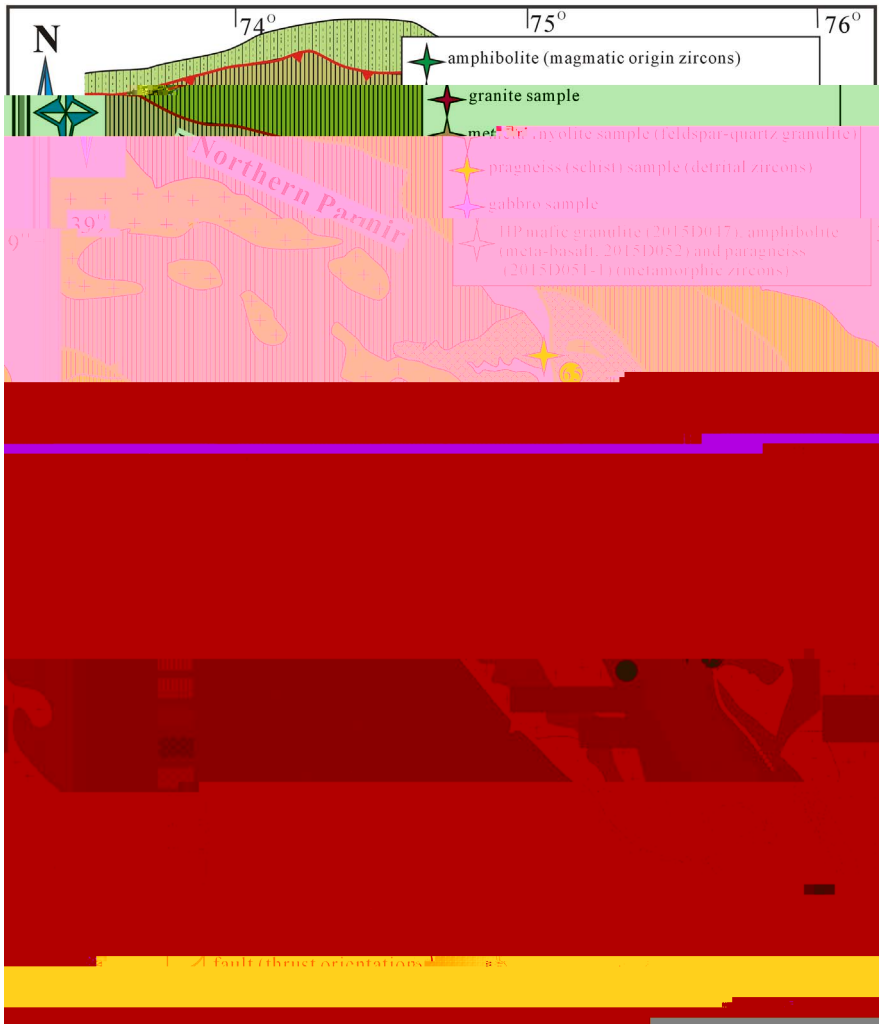

Fig. 2. Sketch geological map of the northeastern section of the Pamir Plateau (see details in the text. Sample locations are shown and the marked number was shortened, i.e., 29 marked in the figure represents 2015D029).

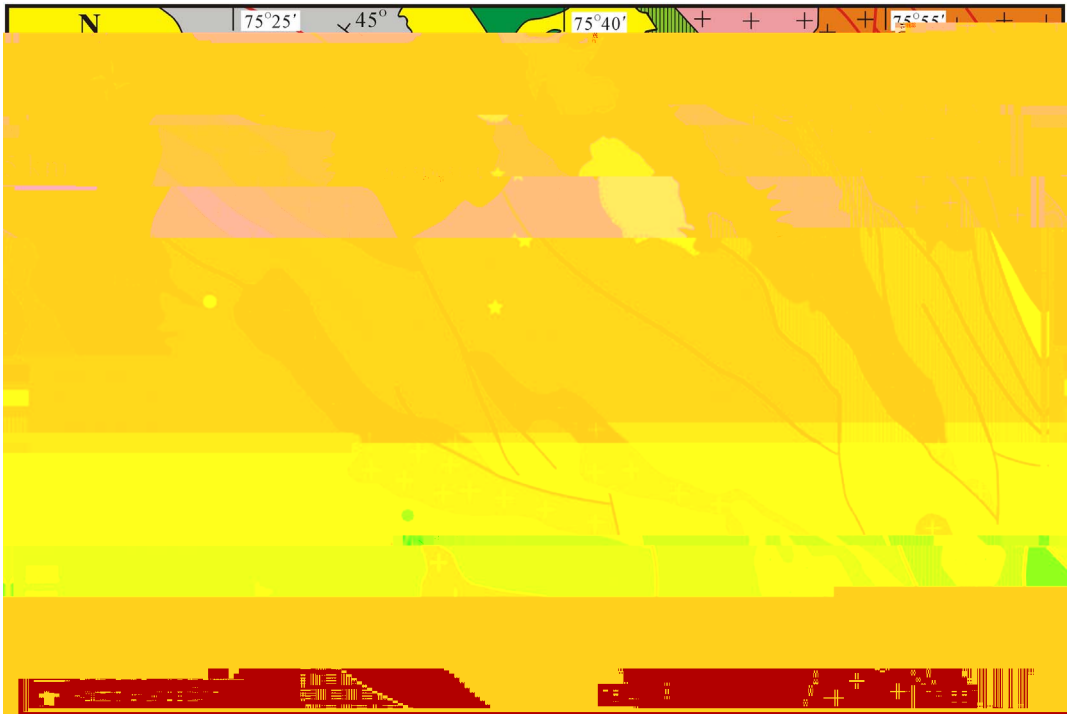

Fig. 3. Geological map of the southern section of the Bulunkuole Group (the Zankan-Laobing iron deposits area).

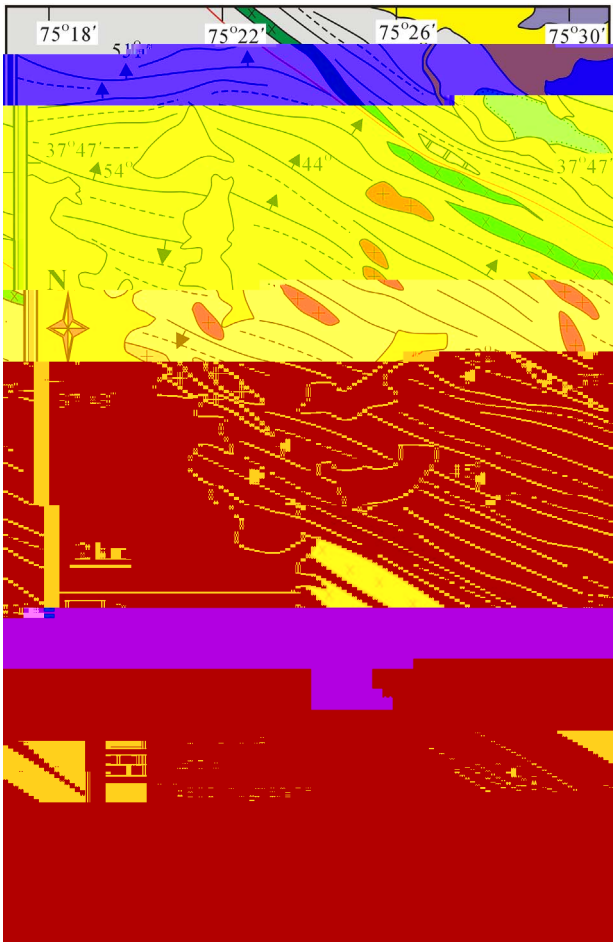

Fig. 4. Geological map at the central section of the Bulunkuole Group.

NW290°–310° and mainly dip to NE at an angle of 30° to 60°. Two distinct rock types could be identified in field and thin section observations, i.e., paragneiss (schist) and orthogneiss. The paragneiss (schist) includes garnet biotite schist, sillimanite-garnet schist, biotite schist (gneiss), and minor marble. The orthogneiss includes amphibolite (Fig. 6c), biotite feldspar-quartz leptynite (meta-rhyolite or meta-volcaniclastic rocks). Two layers of amphibolite, each about several hundred meters thick, were observed in the field (Fig. 6c). High-pressure mafic granulite has been identified nearby to north of this section (Fig. 2, Qu et al., 2007; Yang et al., 2011). On the outcrop, they have typical characteristic 'white-eyes' structure, i.e., the red garnet is surrounded by gray symplectic plagioclases and amphiboles (Fig. 6d). The typical assemblage of high-pressure granulites is garnet (15%–20%), clinopyroxene (20%–30%), plagioclase (20%–30%), hornblende (15%–20%) and minor quartz, rutile, ilmenite, zircon, and titanite. Detailed studies defined a clockwise P-T path of the high-pressure mafic granulite (Qu et al., 2007; Yang et al., 2010). On several outcrops, gneissic gabbro, augen granite and leucogranite sheets of several meters thick and several hundred meters long, occur in parallel within the metamorphic sequences (Fig. 6e).

In the north section of the Bulunkuole Group (represented by the Ziluoyi area), the strata broadly strike in ~W-E direction and dip north at an angle of 30° to 40° (Fig. 6f, amphibolite interlayered with marble). The rock associations in this area are comparable with those of the Zankan-Laobing area, and include amphibolite (meta-basalt), quartz-plagioclase leptynite (meta-rhyolite, Fig. 6g), (garnet-bearing) biotite schist (gneiss), and magnetite layers (Fig. 6h). Early Paleozoic granite plutons intruded into this group (Fig. 5). In line with the iron layers most occurring between meta-bimodal volcanic rocks and meta-clastics or quartzite, the strata in the Ziluoyi area were possibly overturned (Fig. 6h).

Regional mapping and field observations reveal that the rock associations of the Bulunkuole Group in different locations generally resemble each other. Nevertheless, from south to north, foliation strikes gradually change from NW to EW direction. The early Paleozoic granites are mainly distributed along the eastern and northern sides whereas the Mesozoic granites are distributed along the southwestern side.

Thin section observations on the representative rocks are shown in Fig. 7. Garnet biotite schist/gneiss and sillimanite biotite schist/gneiss have medium- to coarse-grained foliated texture and/or porphyroblastic texture, gneissic or schistose structure (Fig. 7a, b). Minerals include sillimanite (1%–10%), garnet (1%–20%, some up to 30%), biotite (15%–35%), muscovite (1%–5%), quartz (40%–60%), and plagioclase (generally < 5%, some up to 15%). Feldspar-quartz leptynite (meta-rhyolite) is composed of 5–10% biotite, 15–20% plagioclase, 10–15% microcline, 35–50% quartz, and minor Ti-Fe oxide (Fig. 7c). Amphibolites outcropping with the leptynite to form a bimodal volcanic series, are fine- to medium- grained, exhibit gneissic structure, and are composed of plagioclase (40–50%), hornblende (40–50%), biotite (5–10%) with occasional quartz (1–5%) and Ti-Fe oxide (3–10%)

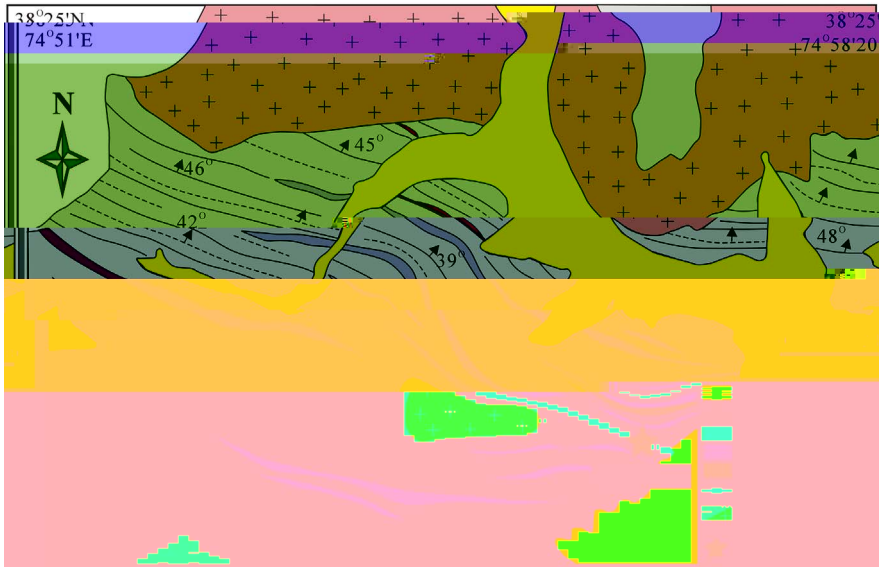

Fig. 5. Geological map at the northern section of the Bulunkuole Group (Ziluoyi iron deposit).

Fig. 6. Representative field photographs of the Bulunkuole Group in NE Pamir. (a) BIF-type iron deposit in Taaxi area (southern section of Bulunkuole Group), the amphibole-bearing magnetite layer occurs between metamorphic bimodal volcanic rocks (amphibolite and feldspar-quartz leptynite) and quartzite (the bedding attitude is shown, southeastward view); (b) metamorphic bimodal volcanic sequence (amphibolite - feldspar-quartz leptynite series) in the southern section of the Bulunkuole Group (northward view); (c) thick layer of amphibolite (metamorphosed from basalt) in central section of the Bulunkuole Group (southeastward view); meta-rhyolite conformably covered by meta-sandstone and biotite schist in southern section of the Bulunkuole Group (the bedding attitude is shown, southeastward view); (d) "white-eyes" structure of the high pressure mafic granulite to north of Tashkorgon County, i.e., the red garnet is surrounded by gray symplectic plagioclases and amphiboles; (e) augen gneissic granite dyke and leucogranite dyke sheets occur in parallel in the central section of the Bulunkuole Group (northeastward view); (f) amphibolite (metamorphosed from basalt) interlayered with marble in northern section of the Bulunkuole Group (Ziluoyi iron deposit, northward view); (g) meta-rhyolite in northern section of Bulunkuole Group (Ziluoyi iron deposit, sample 2015D041); (h) iron layer between bimodal volcanic sequence and meta-clastic

(Fig. 7d). The gneissic gabbro, outcropping as sheet in the Bulunkuole Group, is coarse-grained, and consists of hornblende (50–60%), plagioclase (20–30%), Ti-Fe oxide (2–5%) and minor quartz (< 1%) (Fig. 7e). Hornblende pseudomorphs after clinopyroxene are observed (Fig. 7e). The hornblende magnetite is mainly composed of hornblende (25–40%) and magnetite (55–70%) with minor quartz, biotite and epidote (Fig. 7f).

Fifteen geochronological samples were collected from the Bulunkuole Group. The rock types include garnet biotite quartz schist (paragneiss), mafic granulite, quartz-plagioclase leptynite (meta-

Fig. 7. Representative microphotos of the diverse rocks from the Bulunkuole Group (see details in the text). gt-garnet, bi-biotite, q-quartz, sil-sillimanite, pl-plagioclase, pt.-strip feldspar, hb-hornblende, mt-magnetite.

rhyolite), gneissic granitic dykes, and gneissic gabbro. Five igneous samples and two metamorphic samples were selected for zircon Hf isotope analysis. Rock type, structure, texture, rock-forming minerals, longitude and latitude of each sample are presented in Supplementary Table 1. Sample locations are also shown in Fig. 2.

4. Analytical procedures

Zircon separation was carried out using conventional magnetic and density techniques to concentrate non-magnetic, heavy fractions. Zircon grains were then hand-picked under a binocular microscope. For the zircon U-Pb dating, the grains and zircon standard 91,500 were mounted in epoxy mounts that were then polished to section the crystals in half for analysis. All zircons were documented with transmitted and reflected light micrographs as well as cathodoluminescence (CL) images to reveal their internal structures. Zircon U-Pb ages were analyzed using the LA-ICPMS method at Tianjin Institute of Geology and Mineral Resources, Chinese Geology Survey (CGS). A Neptune MC-ICP-MS coupled with a 193 nm excimer laser ablation system were used to determine zircon U-Pb ages. The laser beam diameter was 35 μm and it was operated with a frequency of 10 Hz. Every set of five sample analyses was followed by analysis of the zircon standard 91,500 and eight sample analyses followed by the zircon standard GJ-1 (Jackson et al., 2004), and the glass standard NIST610 (Hou et al., 2009; Geng et al., 2011). Common Pb was corrected using the method proposed by Andersen (2002). The U-Pb concordia plots were processed with ISOPLOT 3.0 and data are presented with 1σ errors and 95% confidence limits (Ludwig, 2003). The zircon U-Pb age data are listed in Supplementary Table 2.

Analysis of hafnium isotopic ratios of zircon was conducted by LA-MC-ICP-MS at Nanjing FocuMS Technology Co. Ltd. Teledyne Cetac Technologies *An E i* laser-ablation system (Bozeman, Montana, USA) and Nu Instruments *N P s II* MC-ICP-MS (Wrexham, Wales, UK) were combined for the experiments. The 193 nm ArF excimer laser, homogenized by a set of beam delivery systems, was focused on zircon surface with fluence of 6.0 J/cm^2. Ablation protocol employed a spot diameter of 50 μm at 8 Hz repetition rate for 40 s (equating to 320 pulses). Helium was applied as carrier gas to efficiently transport aerosol to MC-ICP-MS. Two standard zircons (including GJ-1, 91,500, Plešovice, Mud Tank, Penglai) were treated as quality control every ten unknown samples. The analytical procedure has been documented in Wu et al. (2006) and Geng et al. (2011). The isotope data are presented in Supplementary Table 3.

5. Analytical results

5.1. i n -P s f r n iss f B n G

Among the five paragneiss or schist samples (2015D034, 2015D043, 2015D044, 2015D045, 2015D065) from the Bulunkuole Group, zircons from four samples resemble each other in appearance except for their variable grain sizes. Most zircons range from 80 μm to 150 μm in length with length to width ratios of 1–3. Some zircons are oval or round, indicating their long-distance transportation, whereas others are euhedral or semi-euhedral. In CL images, they show very different inner features. Some of them exhibit oscillatory zoning, similar to the zircons

crystallized from silicic magma, whereas others show homogenous or wide stripe inner texture, sharing some features of the zircons crystallized from mafic magma (Supplementary Fig. 1). The distinct features of the detrital zircons suggest that they were derived from different sources. Core-mantle texture is occasionally seen in CL images but most mantles are too thin for a single spot analysis. In sample 2015D065, several zircons are oval and have very bright CL images, possibly crystallized during metamorphism (Vavra et al., 1999; Whitehouse and Kamber, 2002), and the analytical results also demonstrated their metamorphic origin according to their very low Th/U ratios and consistent Mesozoic ages (Th/U ratios < 0.05, mean $^{206}Pb/^{238}U$ age = 208 ± 4 Ma, Supplementary Table 2). As for sample 2015D034, intensive metamictization is seen in almost all zircons due to their high uranium contents (see Supplementary Table 1). A few zircons display blurry original euhedral concentric zoning under CL images.

A total of 132 analyses were carried out for the paragneiss/schist samples from the Bulunkuole Group (Supplementary Table 1). According to the results, except for sample 2015D034, most relatively juvenile detrital zircons (< 1.0 Ga) yield concordant $^{206}Pb/^{238}U$ and $^{207}Pb/^{235}U$ ages while the older zircons (> 1.0 Ga) show variable radiogenic lead loss (Fig. 8a, also see Supplementary Fig. 2, the concordia for each sample). We put all the analyses together and illustrate them in Fig. 8b and c, and their concordant ages range from 510 Ma to 1000 Ma. On the age histogram, two peaks at 580 Ma and 795 Ma were observed (Fig. 8c).

5.2. Interpretation of the meta-rhyolite and Bulunkuole Group

Zircons from the meta-rhyolite sample 2015D046 are of columnar forms, transparent and colorless, ranging from 80 to 150 μm in length with length/width ratios of 2–3. According to CL image features, almost all zircon grains display oscillatory zoning, sharing features of the zircons crystallized from silicic magmas (Fig. 9). A small number of zircons have core-mantle texture but the mantle part is too thin for a single spot analysis. Thirty-nine analyses were performed on zircons from this sample. These zircons have Th content of 101–1150 ppm and U content of 203–1484 ppm with Th/U ratios between 0.6 and 1.0. All the analyses yield consistent $^{206}Pb/^{238}U$ ages with a weighted mean age of 515.0 ± 1.7 Ma (MSWD = 0.83) (Fig. 9b).

Zircons from the meta-rhyolite sample 2015D041 share most features with those of sample 2015D046, ranging from 80 μm to 150 μm in length with length to width ratios of 1–2. In CL images, no core-mantle texture is observed (Fig. 9). Twenty-six analyses were obtained and the results are consistent within analytical errors. They have variable Th and U contents but similar Th/U ratios of ~0.6. The weighted mean $^{206}Pb/^{238}U$ age of 508.1 ± 2.1 Ma (N = 26, MSWD = 0.81) (Fig. 10) is interpreted as the crystallization age of the rhyolite.

Zircons from the amphibolite sample 2015D039 are euhedral, transparent, and colorless, ranging from 100 to 200 μm in length with length/width ratios of 2–4. Most zircon grains are homogeneous in CL images (Fig. 9) and a few grains show patchy or fan-like inner texture, sharing the features of the zircons crystallized from mafic magma (Hoskin and Schaltegger, 2001). Twenty-two analyses performed on this sample show that they have Th content of 31–690 ppm and U content of 207–834 ppm and Th/U ratios between 0.8 and 1.2, with the exception of spot 10 that has Th/U ratios < 0.1 and abnormally juvenile $^{206}Pb/^{238}U$ age of 154 Ma. The other 21 analyses yield consistent $^{206}Pb/^{238}U$ ages with a weighted mean age of 518.8 ± 2.0 Ma (MSWD = 0.67) (Fig. 10).

5.3. Interpretation of the augen gneissic granodiorite and Guanzhuang Group

Zircons from the augen gneissic granodiorite sample (2015D050-2) are euhedral and are 80–150 μm long with length to width ratios of 1–2. Euhedral concentric zoning texture is commonly seen, sharing the typical features of the zircons crystallized from granitic magma. Thirty-two analyses were conducted for this sample. They have variable Th and U contents with Th/U ratios ranging from 0.5 to 1.5. All the analyses yield broadly concordant $^{206}Pb/^{238}U$ and $^{207}Pb/^{235}U$ ages. The weighted mean $^{206}Pb/^{238}U$ age of 510.8 ± 2.1 Ma (MSWD = 1.13, Fig. 10) is interpreted as the crystallization age of the augen gneissic granodiorite.

Zircons grains from the gneissic granite sheet (sample 2015D029) are transparent and colorless and

sheet.

Zircons from the gneissic granite (sample 2015D040) are generally colorless, euhedral to sub-euhedral, and range from 100 μm to 200 μm in length with length to width ratios of 2–

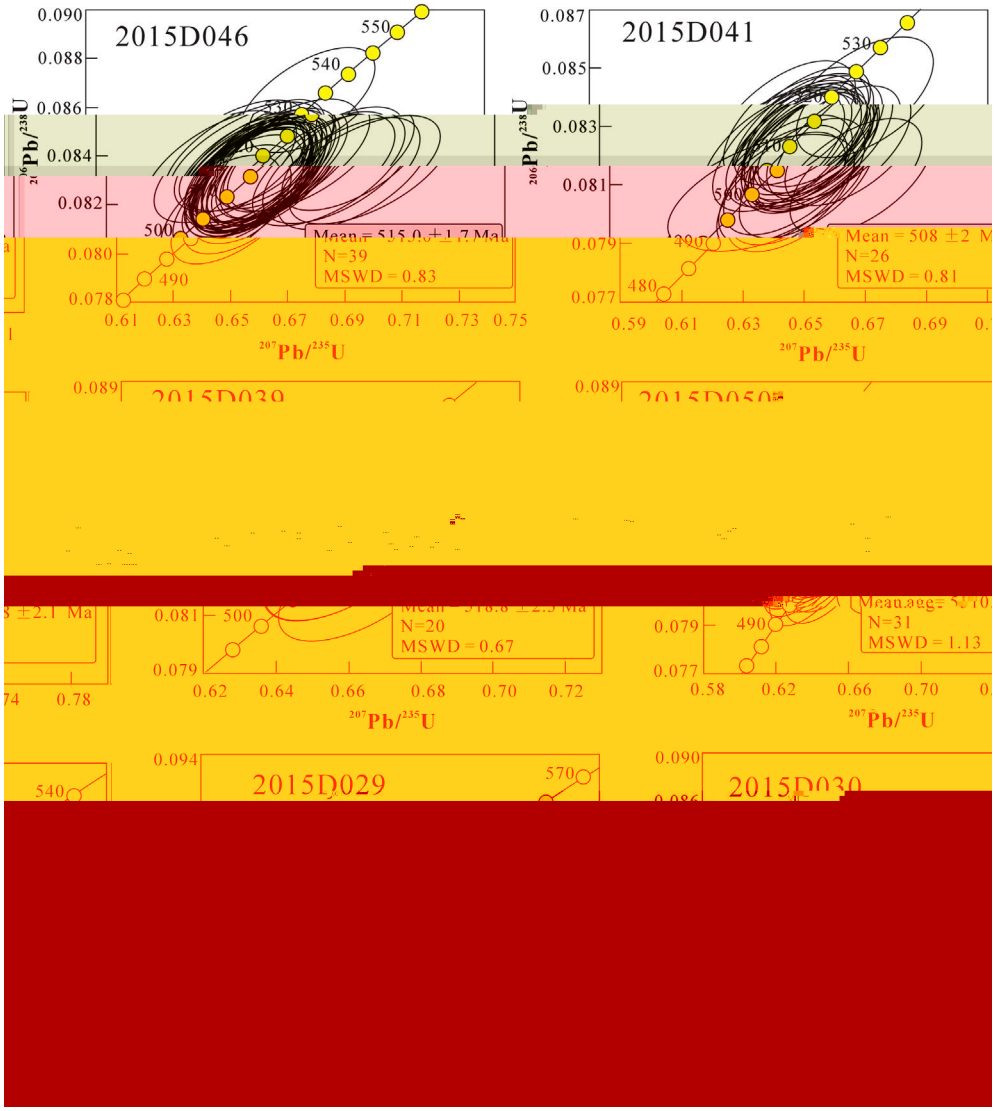

Fig. 10. Concordia of the zircon U-Pb data of the gneissic granulite (meta-rhyolite), gneissic granite sheets, altered gabbros from the Bulunkuole Group (see details in the text).

(southern section), the zircon U-Pb ages of meta-rhyolite and meta-volcaniclastic rocks range from 530 Ma to 520 Ma (Yang et al., 2012; Chen et al., 2013; Zheng et al., 2016), which is consistent with the lower limit of our detrital zircon U-Pb ages (slightly older than 520 Ma) and the ca. 510.8 Ma gneissic granite dykes (sample 2015D050-2) intruding into it. In the central section (Tashkorgon), the age of the feldspar-quartz leptynite (meta-rhyolite, sample 2015D046) yields concordant age of 515.0 ± 1.7 Ma whereas an amphibolite sample yields a concordant age of 518.8 ± 2.3 Ma (2015D039). According to the CL image features and positive zircon εHf(t) values, the analyzed zircons from the amphibolite sample crystallized from mafic magma, although we could not definitely identify its protolith. We tentatively suggest that this amphibolite likely represents a mafic sheet (gabbro or dolerite?) that intruded into the sedimentary sequence at nearly the same time of the deposition of the strata. Thus, the deposition age in the central section of the Bulunkuole Group is constrained between 520 Ma and 510 Ma. In the northern section, the age of the meta-rhyolite sample (sample 2015D041, 508 Ma) is interpreted to represent the deposition age of the volcanic-sedimentary rocks in this area.

Collectively, our results show the Bulunkuole Group was likely deposited in the Cambrian rather than Paleoproterozoic or Triassic (e.g., Robinson et al., 2012). Importantly, the deposition ages became progressively younger from south to north, i.e., from 530–520 Ma in south through 518 Ma in the center to 508 Ma in north. In the eastern section of WKOB, recent studies reveal that the amphibolite-facies metamorphic Saitula Group in the SKT was deposited during the late Neoproterozoic to Cambrian, and its rock associations are also comparable with those of the Bulunkuole Group (Zhang et al., 2017).

We note that a large population of zircons of Pan-Africa ages occurred in the paragneiss/schist from the Bulunkuole Group. According to recent studies, the age spectra of detrital zircons from the Precambrian members in NKT defined several peaks at 1.8 Ga, 1.4 Ga, 0.82–0.80 Ga, 0.78 Ga and 0.75 Ga (Wang et al., 2014; C.L. Zhang et al., 2016). The absence of the Pan-Africa zircons from the Paleozoic rocks in the southern margin of the Tarim Block, as well as the lack of Pan-Africa igneous activities in Tarim, rules out the possibility that the detritus of the Bulunkuole Group was derived from the Tarim Block. Thus, a possible source for these detritus of the Bulunkuole Group is the Gondwana-affinity terranes, such as Lhasa terrane and South Qiangtang terrane (Z.M. Zhang et al., 2012; C.L. Zhang et al., 2012; Lin et al., 2013 and references therein; Angiolini et al., 2015).

6.2. M[illegible] i [illegible] f [illegible] B n [illegible] G

According to field and thin section observations, the metamorphic grade of the Bulunkuole Group is up to amphibolite-facies and even to high-pressure granulite-facies (Qu et al., 2007; Yang et al., 2011). Their inner features revealed by CL images and morphology of the zircons

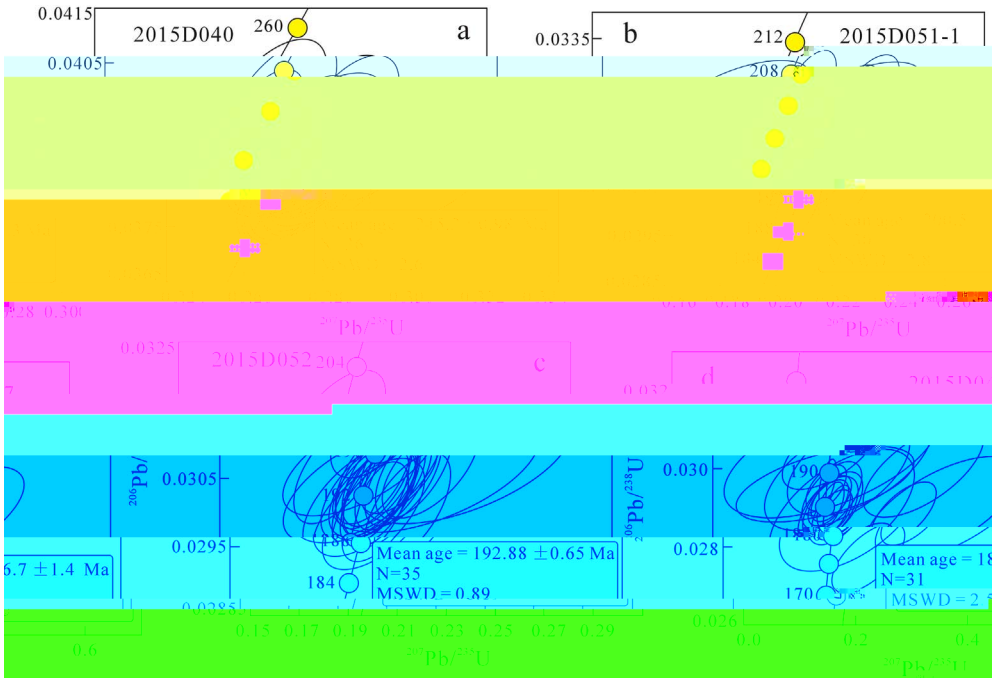

Fig. 11. Concordia of the zircon U-Pb data of the gneissic granite sheet and metamorphic zircons of the paragneiss, amphibolite (meta-basalt) and high-pressure mafic granulite (see details in the text).

from amphibolites (Fig. 9), paragneiss and high-pressure mafic granulite, as well as their Th and U contents (Supplementary Table 2), suggest that their concordant U-Pb ages represent the metamorphic age of the Bulunkuole Group, i.e., at ca. 200–180 Ma (sample 2015D047, 2015D052 and 2015D051-1). Qu et al. (2007) reported a broadly concordant zircon U-Pb age of 177 ± 6 Ma of the HP mafic granulite, which is consistent with our result (186.7 ± 1.4 Ma) within analytical error.

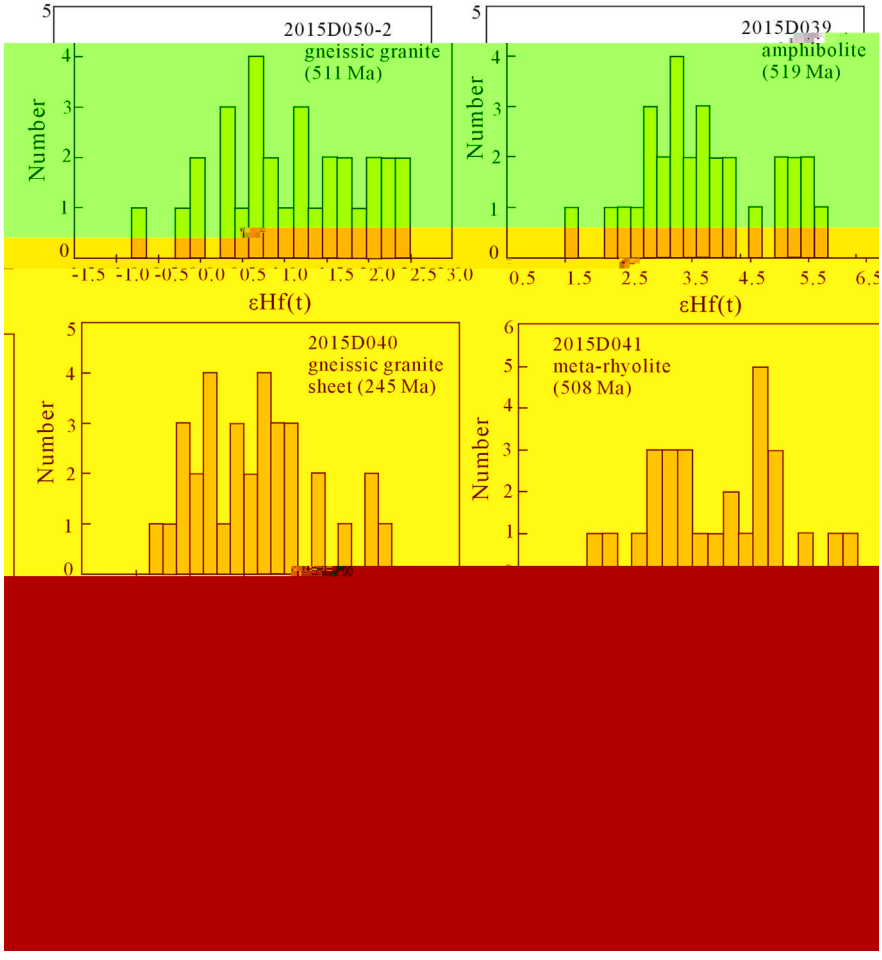

Fig. 12. Histogram of the εHf(t) values of the representative rocks from the Bulunkuole Group (see details in the text).

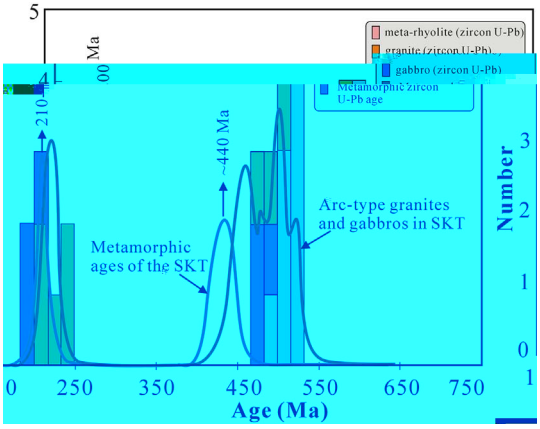

Fig. 13. Histogram of the zircon U-Pb ages of the meta-rhyolite, intrusive rocks and the metamorphic ages of the paragneiss, amphibolite (meta-basalt) and high-pressure mafic granulite.
(Data are from Zhou et al., 1999, 2000; Cui et al., 2006a, 2006b, Liu et al., 2015; Jiang et al., 2002; Zhang et al., 2006, 2007, 2017; Y. Zhang et al., 2016 and references therein and this study).

Yang et al. (2010) suggested the HP granulite facies metamorphism of the Bulunkuole Group took place during 250 Ma and 220 Ma. However, we note that at least one third of their analyses yield discordant $^{206}Pb/^{238}U$ and $^{207}Pb/^{235}U$ ages (see Figs. 5 and 8a in Yang et al., 2010). Moreover, eight analyses of the garnet amphibolite sample yield a weighted mean $^{206}Pb/^{238}U$ age of 180.8 ± 2.4 Ma (see Fig. 8a in Yang et al., 2010), which is consistent with our results. As mentioned above, voluminous arc granites in the Bulunkuole Group emplaced at ca. 240–210 Ma, indicating the subduction continued till at least 210 Ma. Thus, it is reasonable to deduce that the collision and peak metamorphism in NE Pamir took place at ca. 200–180 Ma. This conclusion is consistent with U-Pb geochronology of detrital zircons showing a prominent Early Jurassic population of metamorphic zircon ages with a pronounced peak at 190 Ma in this area (Robinson et al., 2012; Blayney et al., 2016).

Some previous works suggested that the Bulunkuole Group underwent early Paleozoic metamorphism similar to that of the SKT, according to the intrusion of early Paleozoic arc granites into the Bulunkuole Group (Jiang et al., 1999, 2002; Zhang et al., 2003; Ji et al., 2004). However, neither the geochronological data nor the stratigraphic framework favors early Paleozoic metamorphism.

6.3. [illegible]

According to the 1/250,000 geological mapping and our field observations, the Bulunkuole Group is mainly composed of amphibolite-facies metamorphic volcanic-sedimentary sequence with minor marble layers. In line with field observations, the mineral compositions and texture as well as geochemical data (Ji et al., 2004), the protoliths of the amphibolites, feldspar-quartz leptynites and some plagioclase-rich gneiss were basalts, rhyolite and possible volcaniclastic rocks, respectively. On the other hand, the common occurrence of amphibolite layers (meta-basalts) in the Bulunkuole Group shows geochemically deviation from intra-ocean subduction related mafic rocks to arc mafic rocks according to the 1/250,000 mapping (Cui et al., 2006b; Ji et al., 2004). This scenario is very similar with that of the accretionary complex in southern margin of the Altai orogenic belt (Xiao et al., 2009; Ye et al., 2017). We notice that voluminous early Paleozoic granite-granodiorites and minor gabbro sheets intruded the Bulunkuole Group. These granitic intrusions exhibit typical I-type signatures formed in an arc setting (Jiang et al., 1999, 2002). Thus, the volcanic-sedimentary sequence of the Bulunkuole Group and the early Paleozoic intrusions formed an early Paleozoic magmatic accretionary arc system, which is similar to the scenario of the eastern section of the WKOB (Xiao et al., 2002b, 2005; Zhang et al., 2017).

Zircon Hf isotope compositions of the representative rocks from the Bulunkuole Group suggested that the mafic rocks were derived from depleted mantle sources whereas the rhyolites were mainly derived from crustal materials with variable involvements of the depleted mantle-derived mafic magmas as revealed by their slightly positive εHf (t) values of some zircon grains (Iizuka et al., 2017) (Fig. 12). On the other hand, both the early Paleozoic and early Mesozoic granites show slightly negative to positive εHf(t) values. In combination with their geochemical data (Jiang et al., 2002; Jiang et al., 2013; Y. Zhang et al., 2016), we propose that both phases of the granites were formed in arc settings (Vervoort and Kemp, 2016).

6.4. [illegible]

The largest granite pluton emplaced in the Bulunkuole Group is the Konggur Shan pluton, covering > 1200 km^2. It crystallized at ca. 245–210 Ma according to recent zircon U-Pb ages (Robinson et al., 2004; Jiang et al., 2013). Our data also reveal that some gneissic granite dykes emplaced at ca. 240 Ma. The other phase of intrusion is at ca. 510–480 Ma, including the ca. 800 km^2 Datong pluton and several smaller granite plutons with outcrop areas of several tens to more than one hundred square kilometers. It is noteworthy that no intrusive activity during 480 Ma–245 Ma has been identified in the NE Pamir (Fig. 13). Importantly, both the early Mesozoic and early Paleozoic granites show I-type geochemical signatures and most geologists favored arc models for their formation (Jiang et al., 2002; Zhang et al., 2005; Cui et al., 2006a).

6.5. [illegible]

According to our recent work in the eastern section of the WKOB, the southern Kunlun terrane (SKT) is an early Paleozoic accretionary wedge produced by southward subduction of the Proto-Tethys ocean under the Tianshuihai terrane (Fig. 1, TSHT). The subduction possibly began at ca. 530 Ma according to 530–520 Ma gabbro and granodiorite recently identified in TSHT (Hu et al., 2016). In the NE Pamir, the rock association of the Bulunkuole Group suggests that those volcanic-sedimentary sequences likely formed at an arc setting. The broadly coeval volcanic rocks and granites/gabbros emplaced in the Bulunkuole Group (i.e., the volcanic rocks erupted during 530–508 Ma while the granites/gabbros emplaced at 518–480 Ma), also argue for an arc system. Previous geochemical work also demonstrated an arc- affinity of the early Paleozoic granites (Jiang et al., 2002). Thus, we suggest that the Proto-Tethys ocean subducted southward under the TSHT, producing the huge SKT and the NE Pamir accretion wedge in the early Paleozoic (Fig. 14a). This process was geodynamically related to the assemblage of the blocks in northern Tibet and eastern Asia (including the Tarim, Qaidam, South Qiangtang, Yangtze, Indochina, Sibumasu, etc.) to the northern margin of the Gondwana Land (Metcalfe, 2011, 2013; Metcalfe et al., 2017; Li et al., 2017).

In the eastern section of the WKOB, the Proto-Tethys ocean between Tarim (NKT) and the TSHT closed at ca. 440 Ma, as demonstrated by metamorphic zircon and monazite U-Pb ages from paragneiss (Fig. 13, Zhang et al., 2017). The Kuda-Qimantage ophiolite belt represents the suture zone between NKT and SKT. In combination with the commonly seen early Paleozoic orogenic event along the northern Qaidam, Qilian, Qinling, Cathysia and southeastern Asia (see details in Li et al., 2017), we suggest that the final assemblage of the above-mentioned blocks to the Gondwana Land finished at 440–430 Ma. However, along the NE margin of the Pamir Plateau, the following lines of evidence suggest that the early Paleozoic accretionary wedge as represented by the Bulunkuole Group did not amalgamate with NKT or Tarim during late Paleozoic: (1) no early Paleozoic ophiolite has ever been identified along the NE Pamir; (2) neither early Silurian metamorphism (ca.

440 Ma) nor late Silurian to early Devonian post-orogenic intrusions (430–400 Ma) have been documented in this area, and (3) possibly the most important evidence, in western Tarim, the Ordovician-Silurian and the Devonian sedimentary sequences were characterized by shallow marine sedimentary features and the Carboniferous-Permian sequences are mainly platform limestone (Ding et al., 1996). These pre-Mesozoic sequences are unconformably covered by the Jurassic-Cretaceous red molasse. In the NE Pamir, in line with the data presented in this study, the Cambrian Bulunkuole Group shows significant magmatic arc signatures and is intruded by two phases of magmatic rocks; an early Paleozoic phase (500–480 Ma) and an early Mesozoic phase (240–210 Ma). However, no early Paleozoic metamorphism has been identified, and the late Paleozoic sequence in the NE Pamir shows passive continental margin sedimentary features (Ding et al., 1996). Thus, we suggest the proto-Tethys ocean between the Tarim and the NE Pamir did not close until the early Mesozoic as demonstrated by the 200–180 Ma amphibolite facies metamorphism of the Bulunkuole Group (Fig. 14b). This remnant Proto-Tethys ocean was filled by Paleozoic to early Mesozoic sedimentary sequences, similar to the scenario of the Junggar basin in the Central Asia Orogenic belt (Xiao et al., 2009).

There is a ~110 Ma time gap between the final assemblage of Gondwana and its breakup. Since late Carboniferous, the breakup of the Gondwana induced the formation of the Paleo-Tethys Ocean and consumption of the Paleo-Tethys Ocean led to the assemblage of the Pangea during Carboniferous to Triassic (Metcalfe, 2011, 2013; Metcalfe et al., 2017). In this process, northward subduction of the Paleo-Tethys Ocean along the southern margin of the NE Pamir and the TSHT likely began at ca. 240 Ma in line with the earliest Mesozoic arc granites intruding into the Bulunkuole Group and the TSHT (Fig. 14c). During 240–200 Ma, voluminous granites were emplaced along the Kongur Shan mountain in the NE Pamir, the TSHT, and the southern belt of the South Kunlun terrane, suggesting that northward subduction continued until at least 200 Ma (Fig. 14c). In the eastern section of the WKOB, closure of the Paleo-Tethys Ocean took place at ca. 205–200 Ma as demonstrated by monazite U-Pb ages from the metamorphic rocks along the Kangxiwa fault and the lower Jurassic molasse unconformably overlying on the pre-Jurassic sequences in TSHT (Zhang et al., 2017). While in the western section, the 200–180 Ma amphibolite- to granulite-facies metamorphism of the Bulunkuole Group represents the collision between the Central Pamir and NE Pamir (Fig. 14d). Thus, we conclude that the closure process of the Paleo-Tethys Ocean propagated from east to west with final closure at ca. 180 Ma, which is consistent with stratigraphic data such as an un-

(3) The closure of the Paleo-Tethys Ocean propagated gradually from east to west. The accretion between the Central Pamir and the NE Pamir occurred at ca. 180 Ma, slightly later than the closure of the ocean basin between the TSHT and the Karakorum terrane (ca. 200 Ma).

Supplementary data to this article can be found online at https://doi.org/10.1016/j.tecto.2017.11.036.

Acknowledgements

We sincerely thank Mr. Wen-Hua Ji for his help with the field work and supplying the 1/50,000 and 1/25,000 geological maps and related scientific reports. We are grateful to Hong-Ying Zhou for his assistance with LA-ICP-MS zircon dating, and to Prof. Jian-Feng Gao for his help with zircon Lu-Hf isotope analyses. We are grateful to Prof. Alexander C. Robinson and Prof. Wen-Jiao Xiao for their critical and insightful reviews that greatly improved the quality of this paper. This project is funded by the National 305 Project of China (2015BAB05B0X-03) and the Fundamental Research Fund for Central Universities (B16020127).

References

Andersen, T., 2002. Correction of common lead in U-Pb analyses that do not report ^{204}Pb. Chem. Geol. 192, 59–79.
Angiolini, L., Zanchi, A., Zanchetta, S., Nicora, A., Vezzoli, G., 2013. The Cimmerian geopuzzle: new data from South Pamir. Terra Nova 25, 352–360.
Angiolini, L., Zanchi, A., Zanchetta, S., Nicora, A., Vuolo, I., Berra, F., Henderson, C., Malaspina, N., Rettori, R., Vachard, D., Vezzoli, G., 2015. From rift to drift South Pamir (Tajikistan): Permian evolution of a Cimmerian terrane. J. Asian Earth Sci. 102, 146–169.
Blayney, T., Najman, Y., Dupont-Nivet, G., Carter, A., Millar, I., Garzanti, E., Sobel, E.R., Rittner, M., Andò, S., Guo, Z.J., Vezzoli, G., 2016. Indentation of the Pamirs with respect to the northern margin of Tibet: constraints from the Tarim basin sedimentary record. Tectonics 35, 2345–2369.
Boulin, J., 1988. Hercynian and Eocimmerian events in Afghanistan and adjoining regions. Tectonophysics 148, 253–278.
Burtman, V.S., 2010. Tien Shan, Pamir, and Tibet: history and geodynamics of phanerozoic oceanic basins. Geotectonics Engl. Transl. 44, 388–404.
Burtman, V.S., Molnar, P., 1993. Geological and geophysical evidence for deep subduction of continental crust beneath the Pamir. Spec. Pap. Geol. Soc. Am. 281 (76 pp.).
Chen, D.H., Wu, Y.Z., Li, W.M., Wang, X.A., Qiao, G.B., Zhao, X.J., 2013. Geological characteristics and genesis of the iron deposits in the Taxkorgan Area, West Kunlun. Geotecton. Metallog. 37, 671–684 (in Chinese with English abstract).
Cui, J.T., Wang, J.C., Bian, X.W., Zhu, H.P., Yang, K.J., 2006a. Geological characteristics of Early Paleozoic amphibolite and tonalite in northern Kangxiwar, West Kunlun, China and their zircon SHRIMP U-Pb dating. Geol. Bull. China 25, 1441–1449 (in Chinese with English abstract).
Cui, J.T., Bian, X.W., Wang, J.C., Yang, K.J., Zhu, H.P., Zhang, J.L., 2006b. Discovery of an unconformity between the Lower Silurian and Middle Devonian in the Tianshuihu area, southern Kangxiwar, West Kunlun, China. Geol. Bull. China 25, 1437–1440 (in Chinese with English abstract).
Cui, J.T., Bian, X.W., Wang, G.B., 2006c. Geological composition and evolution of the western Kunlun. Geol. Shaanxi 24, 1–11.
Ding, D.G., Tang, L.J., Qian, Y.X., 1996. Formation and Tectonic Evolution of the Tarim Basin. Hohai University Press House, pp. 70–133 (in Chinese with English abstract).
Geng, J.Z., Li, H.K., Zhang, J., Zhang, Y.Q., 2011. Zircon Hf isotope analysis by means of LA-MC-ICP-MS. Geol. Bull. China 30, 1508–1513 (in Chinese with English abstract).
Han, F.L., Cui, J.T., Ji, W.H., Li, H.P., Hao, J.W., 2001. Discussion of orogenics of the Western Kunlun mountains during the Caledonian orogeny. Geol. Shaanxi 19, 8–18 (in Chinese with English abstract).
Han, F.L., Cui, J.T., Ji, W.H., Li, H.P., Hao, J.W., 2002. Discovery of the Qimanyute ophiolite and its geological significance. Geol. Bull. China 21, 573–578 (in Chinese with English abstract).
Han, F.L., Cui, J.T., Ji, W.H., Hao, J.W., Meng, Y., 2004. New results and major progress in the regional geological survey of the Yutian County and Bolike sheets. Geol. Bull. China 23, 555–559 (in Chinese with English abstract).
Hoskin, P.W., Schaltegger, U., 2001. The composition of zircon and igneous and metamorphic petrogenesis. Rev. Mineral. Geochem. 53, 25–104.
Hou, K.J., Li, Y.H., Tian, Y.R., 2009. In situ U–Pb zircon dating using laser ablation multi ion counting-ICP-MS. Miner. Depos. 28, 481–492 (in Chinese with English abstract).
Hu, J., Wang, H., Huang, C.Y., Tong, L.X., Mu, S.L., Qiu, Z.W., 2016. Geological characteristics and age of the Dahongliutan Fe-ore deposit in the Western Kunlun orogenic belt, Xinjiang, northwestern China. J. Asian Earth Sci. 116, 1–25.
Iizuka, T., Yamaguchi, T., Itano, K., Hibiya, Y., Suzuki, K., 2017. What Hf isotopes in zircon tell us about crust–mantle evolution. Lithos 274-275, 304–327.
Jackson, S.E., Pearson, N.J., Griffin, W.L., Belousova, E.A., 2004. The application of laser ablation-inductively coupled plasma-mass spectrometry (LA–ICP-MS) to in situ U–Pb zircon geochronology. Chem. Geol. 211, 47–69.
Ji, W.H., Han, F.L., Wang, J.C., Zhang, J.L., 2004. Composition and geochemistry of the Subashi ophiolite mélange in the Western Kunlun and its geological significance. Geol. Bull. China 23, 1196–1201 (in Chinese with English abstract).
Ji, W.H., Li, R.S., Chen, S.J., He, S.P., Zhao, Z.M., Bian, X.W., Zhu, H.P., Cui, J.G., Ren, J.G., 2011. The discovery of Palaeoproterozoic volcanic rocks in the Bulunkuoler Group from the Tianshuihai Massif in Xinjiang of Northwest China and its geological significance. Sci. China (D-series) 54, 61–72.
Jiang, Y.H., Rui, X.J., He, J.R., Guo, K.Y., Yang, W.Z., 1999. Tectonic type of Caledonian granitoids and tectonic significance in the west Kunlun Mts. Acta Petrol. Sin. 15, 105–115 (in Chinese with English abstract).
Jiang, Y.H., Jiang, S.Y., Ling, H.F., Zhou, X.R., Rui, X.J., Yang, W.Z., 2002. Petrology and geochemistry of shoshonitic plutons from the western Kunlun orogenic belt, northwestern Xinjiang, China: implications for granitoid geneses. Lithos 63, 165–187.
Jiang, Y.H., Jia, R.Y., Liu, Z., Liao, S.Y., Zhao, P., Zhou, Q., 2013. Origin of Middle Triassic highK calc-alkaline granitoids and their potassic microgranular enclaves from the western Kunlun orogen, northwest China: a record of the closure of Paleo-Tethys. Lithos 156–159, 13–30.
Li, S.Z., Zhao, S.J., Liu, X., Cao, H., Yu, S., Li, X.Y., Somerville, I., Yu, S.Y., 2017. Closure of the Proto-Tethys Ocean and Early Paleozoic amalgamation of microcontinental blocks in East Asia. Earth-Sci. Rev In press. at website. https://doi.org/10.1016/j.earscirev.2017.01.011.
Lin, Y.H., Zhang, Z.M., Dong, X., Shen, K., Lu, X., 2013. Precambrian evolution of the Lhasa terrane, Tibet: constraint from the zircon U–Pb geochronology of the gneisses. Precambrian Res. 237, 664–677.
Liu, Z., Jiang, Y., Jia, R., Zhao, P., Zhou, Q., 2015. Origin of Late Triassic high-K calcalkaline granitoids and their potassic microgranular enclaves from the western Tibet Plateau, northwest China: implications for Paleo-Tethys evolution. Gondwana Res. 27, 326–341.
Ludwig, K.R., 2003. In: Ludwig, Kenneth R. (Ed.), User's Manual for Isoplot 3.00: A Geochronological Toolkit for Microsoft Excel.
Matte, Ph., Tapponnier, P., Arnaud, N., Bourjot, L., Avouac, J.P., Vidal, Ph., Liu, Q., Pan, Y.S., Wang, Y., 1996. Tectonics of Western Tibet, between the Tarim and the Indus. Earth Planet. Sci. Lett. 142, 311–330.
Mattern, F., Schneider, W., 2000. Suturing of the Proto- and Paleo-Tethys oceans in the Western Kunlun (Xijiang, China). J. Asian Earth Sci. 18, 637–650.
Metcalfe, I., 2011. Tectonic framework and Phanerozoic evolution of Sundaland. Gondwana Res. 19, 3–21.
Metcalfe, I., 2013. Gondwana dispersion and Asian accretion: Tectonic and palaeogeographic evolution of eastern Tethys. J. Asia Earth Sci. 66, 1–33.
Metcalfe, I., Henderson, C.M., Wakita, K., 2017. Lower Permian conodonts from Palaeo-Tethys Ocean Plate Stratigraphy in the Chiang Mai-Chiang Rai Suture Zone, northern Thailand. Gondwana Res. 44, 54–66.
Pan, Y.S., 1996. Geological Evolution of the Karakorum and Kunlun Mountains. Seismological Press, Beijing, pp. 34–78.
Pan, Y.S., Wang, Y., 1994. Discovery and evidence of the Fifth Suture Zone of Qinghai–Tibetan Plateau. Acta Geophys. Sin. 37, 241–250 (in Chinese with English abstract).
Pashkov, B.R., Budanov, V.I., 1990. Tectonics of the SW-SE Pamir junction. Geotectonics 24, 246–253.
Qu, J.F., Zhang, L.F., Ai, Y.L., Lu, Z., Wang, J.P., Zhou, H., Wang, S.Y., 2007. High-pressure granulite from Western Kunlun, northwestern China: its metamorphic evolution, zircon SHRIMP U-Pb ages and tectonic implication. Sci. China D-series 50, 961–971.
Robinson, A.C., 2009. Geologic offsets across the northern Karakorum fault: implications for its role and terrane correlations in the western Himalayan Tibetan orogen. Earth Planet. Sci. Lett. 279, 123–130.
Robinson, A.C., Owen, L.A., Chen, J., Schoenbohm, L.M., Hedrick, K.A., Blisniuk, K., Sharp, W.D., Imrecke, D.B., Li, W., Yuan, Z., Caffee, M.W., Mertz-Kraus, R., 2015. No late Quaternary strike-slip motion along the northern Karakoram fault. Earth Planet. Sci. Lett. 409, 290–298.
Robinson, A.C., Owen, L.A., Chen, J., Schoenbohm, L.M., Hedrick, K.A., Blisniuk, K., Sharp, W.D., Imrecke, D.B., Li, W., Yuan, Z., Caffee, M.W., Mertz-Kraus, R., 2016. Response to comment on “No late Quaternary strike-slip motion along the northern Karakoram fault”. Earth Planet. Sci. Lett. 443, 220–223.
Robinson, A.C., Yin, A., Manning, C.E., Harrison, T.M., Zhang, S.-H., Wang, X.-F., 2004. Tectonic evolution of the northeastern Pamir: constraints from the northern portion of the Cenozoic Kongur Shan extensional system. Geol. Soc. Am. Bull. 116, 953–974.
Robinson, A.C., Yin, A., Manning, C.E., Harrison, T.M., Zhang, S.-H., Wang, X.-F., 2007. Cenozoic evolution of the eastern Pamir: implications for strain accommodation mechanisms at the western end of the Himalayan-Tibetan orogen. Geol. Soc. Am. Bull. 119, 882–896.
Robinson, A.C., Ducea, M., Lapen, T.J., 2012. Detrital zircon and isotopic constraints on the crustal architecture and tectonic evolution of the northeastern Pamir. Tectonics 31, 1–16.
Rutte, D., Ratschbacher, L., Schneider, S., Stübner, K., Stearns, Gulzar M.A., Hacker, B.R., 2017. Building the Pamir-Tibetan Plateau—crustal stacking, extensional collapse, and lateral extrusion in the Central Pamir: 1. Geometry and kinematics. Tectonics 36, 1–43.
Schwab, M., Ratschbacher, L., Siebel, W., Williams, M.M., Minaev, V., Lutkov, V., Chen, F., Stanek, K., Nelson, B., Frisch, W., Wooden, J.L., 2004. Assembly of the Pamirs: age and origin of magmatic belts from the southern Tien Shan to the southern Pamirs and their relation to Tibet. Tectonics 23, 1–31.
Tapponnier, P., Mattauer, M., Proust, F., Cassaigneau, C., 1981. Mesozoic ophiolites, sutures, and large-sale tectonic movements in Afghanistan. Earth Planet. Sci. Lett. 52, 355–371.
Valli, F., Leloup, P.H., Paquette, J.L., et al., 2008. New U/Pb constraints on timing of

shearing and long-term slip-rate on the Karakorum fault. Tectonics 27, 1–33.
Vavra, G., Schmid, R., Gebauer, D., 1999. Internal morphology, habit and U–Th–Pb microanalysis of amphibole to granulite facies zircon: geochronology of the Ivren Zone (Southern Alps). Contrib. Mineral. Petrol. 134, 380–404.
Vervoort, J., Kemp, A.I.S., 2016. Clarifying the zircon Hf isotope record of crust–mantle evolution. Chem. Geol. 425, 65–75.
Wang, C., Wang, Y.H., Liu, L., He, S.P., Li, R.S., Li, M., Yang, W.Q., Cao, Y.-T., Meert, J.G., Shi, C., 2014. The Paleoproterozoic magmatic–metamorphic events and cover sediments of the Tiekelik Belt and their tectonic implications for the southern margin of the Tarim Craton, northwestern China. Precambrian Res. 254, 210–225.
Whitehouse, M.J., Kamber, B.S., 2002. On the overabundance of light rare earth elements in terrestrial zircons and its implication for Earth's earliest magmatic differentiation. Earth Planet. Sci. Lett. 204, 333–346.
Wu, F.Y., Yang, Y.H., Xie, L.W., Yang, J.H., Xu, P., 2006. Hf isotopic compositions of the standard zircons and baddeleyites used in U–Pb geochronology. Chem. Geol. 234, 105–126.
Xiao, W.J., Windley, B.F., Hao, J., Li, J.L., 2002a. Arc-ophiolite obduction in the western Kunlun range (China): implications for the Palaeozoic evolution of central Asia. J. Geol. Soc. 159, 517–528.
Xiao, W.J., Windley, B.F., Chen, H.L., Zhang, G.C., Li, J.L., 2002b. Carboniferous-Triassic subduction and accretion in the western Kunlun, China: implications for the collisional and accretionary tectonics of the northern Tibetan plateau. Geology 30, 295–298.
Xiao, W.J., Windley, B.F., Liu, D.Y., Jian, P., Liu, C.Z., Yuan, C., Sun, M., 2005. Accretionary tectonics of the western Kunlun orogen, China: a Paleozoic-Early Mesozoic, long-lived active continental margin with implications for the growth of southern Eurasia. J. Geol. 113, 687–705.
Xiao, W.J., Windley, B.F., Yuan, C., Sun, M., Han, C.M., Lin, S.F., Chen, H.L., Yan, Q.R., Liu, D.Y., Qin, K.Z., Li, J.Y., Sun, S., 2009. Paleozoic multiple subduction-accretion process of the southern Altaids. Am. J. Sci. 309, 221–270.
Xinjiang, BGMR, 1993. Regional Geology of the Xinjiang Uygur Autonomous Region. Geological Publishing House, Beijing, pp. 155–231 (in Chinese).
Yang, W.Q., Liu, L., Cao, Y.T., Wang, C., He, S.P., Li, R.S., Zhu, X.H., 2010. Geochronological evidence of Indosinian (high-pressure) metamorphic event and its tectonic significance in Taxkorgan area of the Western Kunlun Mountains, NW China. Sci. China D-series 53, 1455–1459.
Yang, W.Q., Liu, L., Cao, Y.T., Wang, C., He, S.P., Li, R.S., Zhu, X.H., 2011. Geochronological evidence of Indosinian (high-pressure) metamorphic event and its tectonic significance in Taxkorgan area of the Western Kunlun Mountains, NW China. Sci. China D-series 53, 1445–1459.
Yang, C.H., Chen, C.J., Cao, X.Z., 2012. The discovery of the Pamir-type iron deposits in Taxkorgan area of Xinjiang and its geological significance. Geol. Bull. China 31, 549–557 (in Chinese with English abstract).
Ye, X.T., Zhang, C.L., Zou, H.B., Yao, C.Y., Dong, Y.G., 2017. Age and geochemistry of the Zhaheba ophiolite complex in eastern Junggar of the Central Asian Orogenic Belt (CAOB): implications for the accretion process of the Junggar terrane. Geol. Mag. 154, 419–440.
Yin, A., Harrison, T.M., 2000. Geologic evolution of the HimalayanTibetan Orogen. Annu. Rev. Earth Planet. Sci. 28, 211–280.
Zanchi, A., Gaetani, M., 2011. The geology of the Karakoram range, Pakistan: the new 1:100,000 geological map of Central-Western Karakoram. Italy J. Geosci. 130, 161–262.
Zanchi, A., Poli, S., Fumagalli, P., Gaetani, M., 2000. Mantle exhumation along the Tirich Mir Fault Zone, NW Pakistan: pre-mid-cretaceous accretion of the Karakoram terrane to the Asian margin. In: Khan, M.A., et al. (Eds.), Tectonics of the Nanga Parbat Syntaxis and the Western Himalaya. 170. Geological Society London Special Publications, pp. 219–236.
Zhang, C.L., Shen, J.L., Wang, A.G., Zhao, Y., 2003. Caledonian low-temperature granulite-facies metamorphism in the West Kunlun Orogenic Belt-SHRIMP geochronological evidence from zircons. Chin. J. Geochem. 22, 345–351.
Zhang, C.L., Yu, H.F., Shen, J.L., Dong, J.G., Ye, H.M., Guo, K.Y., 2004. Zircon SHRIMP age determination of the giant-crystal gabbro and basalt in Kuda, west Kunlun: dismembering of the Kuda ophiolite. Geol. Rev. 50, 639–643 (in Chinese with English abstract).
Zhang, C.L., Yu, H.M., Wang, A.G., Guo, K.Y., 2005. Dating of Triassic granites in the Western Kunlun Mountains and its tectonic significance. Acta Geol. Sin. 79, 645–652 (in Chinese with English abstract).
Zhang, C.L., Yu, H.F., Ye, H.M., Wang, A.G., 2006. Aoyitake plagiogranite in western Tarim Block, NW China: age, geochemistry, petrogenesis and its tectonic implications. Sci. China (Series D) 49, 1121–1134.
Zhang, C.L., Lu, S.N., Yu, H.F., Ye, H.M., 2007. Tectonic evolution of Western Orogenic belt: evidences from zircon SHRIMP and LA-ICP-MS U–Pb ages. Sci. China (Series D) 50, 1–12.
Zhang, Z.M., Dong, X., Santosh, M., Liu, F., Wang, W., Yiu, F., He, Z.Y., Shen, K., 2012. Petrology and geochronology of the Namche Barwa Complex in the eastern Himalayan syntaxis, Tibet: constraints on the origin and evolution of the northeastern margin of the Indian Craton. Gondwana Res. 21, 123–137.
Zhang, C.L., Santosh, M., Zou, H.B., Xu, Y.G., Zhou, G., Dong, Y.G., Ding, R.F., Wang, H.Y., 2012. Revisiting the “Irtish tectonic belt”: implications for the Paleozoic evolution of the Altaid orogen. J. Asian Earth Sci. 52, 117–133.
Zhang, C.L., Zou, H.B., Li, H.K., Wang, H.Y., 2013. Tectonic framework and evolution of the Tarim Block in NW China. Gondwana Res. 23, 1306–1315.
Zhang, Y., Niu, Y.L., Hu, Y., Liu, J.J., Ye, L., Kong, J.J., Duan, M., 2016. The syncollisional granitoid magmatism and continental crust growth in the West Kunlun Orogen, China – evidence from geochronology and geochemistry of the Arkarz pluton. Lithos 245, 191–204.
Zhang, C.L., Ye, X.T., Zou, H.B., Chen, X.Y., 2016. Neoproterozoic sedimentary basin evolution in southwestern Tarim, NW China: new evidence from field observations, detrital zircon U–Pb ages and Hf isotope compositions. Precambrian Res. 280, 31–45.
Zhang, C.L., Zou, H.B., Ye, X.T., Chen, X.Y., 2017. Tectonic evolution of the eastern section of Western Kunlun Orogenic Belt at the northern margin of the Tibetan Plateau: new evidence from field observations and geochronology. Geosci. Front (under review).
Zheng, M.T., Zhang, L.C., Zhu, M.T., 2016. Geological characteristics, formation age and genesis of the Kalaizi Ba-Fe deposit in West Kunlun. Earth Sci. Front. 23, 531–542 (in Chinese with English abstract).
Zhou, H., Li, J.L., Hou, Q.L., Xiao, W.J., Chen, H.H., 1999. A large-scale ductile shear zone in Kudi, West Kunlun. Chin. Sci. Bull. 142, 1774–1776.
Zhou, H., Chu, Z.Y., Li, J.L., Hou, Q.L., Wang, Z.H., Fang, A.M., 2000. $^{40}Ar/^{39}Ar$ dating of ductile shear zone in Kuda, west Kunlun, Xinjiang. Sci. Geol. Sin. 35, 233–239 (in Chinese with English abstract).